

Measurement of the Form-Factor Slopes for the Decay $K_L \rightarrow \pi^\pm e^\mp \nu$ with the KLOE Detector

The KLOE Collaboration

F. Ambrosino^e, A. Antonelli^b M. Antonelli^{b,1}, C. Bacciⁱ,
P. Beltrame^c, G. Bencivenni^b, S. Bertolucci^b, C. Bini^g,
C. Bloise^b, V. Bocci^g, F. Bossi^b, D. Bowring^a, P. Branchiniⁱ,
R. Caloi^g, P. Campana^b, G. Capon^b, T. Capussela^e,
F. Ceradiniⁱ, S. Chi^b, G. Chiefari^e, P. Ciambrone^b,
S. Conetti^a, E. De Lucia^b, A. De Santis^g, P. De Simone^b,
G. De Zorzi^g, S. Dell'Agnello^b, A. Denig^c, A. Di Domenico^g,
C. Di Donato^e, S. Di Falco^j, B. Di Miccoⁱ, A. Doria^e,
M. Dreucci^{b,2}, G. Felici^b, A. Ferrari^c, M. L. Ferrer^b,
G. Finocchiaro^b, S. Fiore^g, C. Forti^b, P. Franzini^g, C. Gatti^{b,3},
P. Gauzzi^g, S. Giovannella^b, E. Gorini^d, E. Grazianiⁱ,
M. Incagli^j, W. Kluge^c, V. Kulikov^m, F. Lacava^g,
G. Lanfranchi^b, J. Lee-Franzini^{b,k}, D. Leone^c, M. Martini^b,
P. Massarotti^e, W. Mei^b, S. Meola^e, S. Miscetti^b,
M. Moulson^b, S. Müller^c, F. Murtas^b, M. Napolitano^e,
F. Nguyenⁱ, M. Palutan^b, E. Pasqualucci^g, A. Passeriⁱ,
V. Patera^{b,f}, F. Perfetto^e, L. Pontecorvo^g, M. Primavera^d,
P. Santangelo^b, E. Santovetti^h, G. Saracino^e, B. Sciascia^b,
A. Sciubba^{b,f}, F. Scuri^j, I. Sfiligoi^b, T. Spadaro^b, M. Testa^g,
L. Tortoraⁱ, P. Valente^b, B. Valeriani^c, G. Venanzoni^b,
S. Veneziano^g, A. Ventura^d, R. Versaci^c, G. Xu^{b,ℓ},

^a*Physics Department, University of Virginia, Charlottesville, VA, USA.*

^b*Laboratori Nazionali di Frascati dell'INFN, Frascati, Italy.*

^c*Institut für Experimentelle Kernphysik, Universität Karlsruhe, Germany.*

^d*Dipartimento di Fisica dell'Università e Sezione INFN, Lecce, Italy.*

^e*Dipartimento di Scienze Fisiche dell'Università "Federico II" e Sezione INFN,
Napoli, Italy*

^f*Dipartimento di Energetica dell'Università "La Sapienza", Roma, Italy.*

^g*Dipartimento di Fisica dell'Università "La Sapienza" e Sezione INFN, Roma,
Italy.*

^h*Dipartimento di Fisica dell'Università "Tor Vergata" e Sezione INFN, Roma, Italy.*

ⁱ*Dipartimento di Fisica dell'Università "Roma Tre" e Sezione INFN, Roma, Italy.*

^j*Dipartimento di Fisica dell'Università e Sezione INFN, Pisa, Italy.*

^k*Physics Department, State University of New York at Stony Brook, NY, USA.*

^ℓ*Permanent address: Institute of High Energy Physics, CAS, Beijing, China.*

^m*Permanent address: Institute for Theoretical and Experimental Physics, Moscow, Russia.*

¹ Corresponding author: Mario Antonelli INFN - LNF, Casella postale 13, 00044 Frascati (Roma), Italy; tel. +39-06-94032728, e-mail mario.antonelli@lnf.infn.it

² Corresponding author: Marco Dreucci INFN - LNF, Casella postale 13, 00044 Frascati (Roma), Italy; tel. +39-06-94032696, e-mail marco.dreucci@lnf.infn.it

³ Corresponding author: Claudio Gatti INFN - LNF, Casella postale 13, 00044 Frascati (Roma), Italy; tel. +39-06-94032727, e-mail claudio.gatti@lnf.infn.it

Abstract

We present a measurement of the K - π vector current form-factor parameters for the decay $K_L \rightarrow \pi^\pm e^\mp \nu$. We use 328 pb⁻¹ of data collected in 2001 and 2002, corresponding to ~ 2 million K_{e3} events. Measurements of semileptonic form factors provide information about the dynamics of the strong interaction and are necessary for evaluation of the phase-space integral I_K^e needed to measure the CKM matrix element $|V_{us}|$ for $K_L \rightarrow \pi^\pm e^\mp \nu$ decays. Our result is $\lambda_+ = (28.6 \pm 0.5 \pm 0.4)10^{-3}$ for a linear fit, and $\lambda'_+ = (25.5 \pm 1.5 \pm 1.0)10^{-3}$, $\lambda''_+ = (1.4 \pm 0.7 \pm 0.4)10^{-3}$ for a quadratic fit.

key words: ke3 form factor

PACS: 13.20.Eb

1 Introduction

Semileptonic kaon decays, $K_L \rightarrow \pi^\pm \ell^\mp \nu$, (Fig. 1) offer possibly the cleanest way to obtain an accurate value of the Cabibbo angle, or better, V_{us} . Since $K \rightarrow \pi$ is a $0^- \rightarrow 0^-$ transition, only the vector part of the weak current has a nonvanishing contribution. The transition is therefore protected by the Ademollo-Gatto theorem against SU(3) breaking corrections to lowest order. At present, the largest uncertainty in calculating V_{us} from the decay rate, is due to the difficulties in computing the matrix element $\langle \pi | j_\mu | K \rangle$. In the

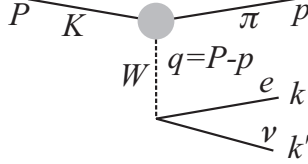


Fig. 1. Amplitude for $K_L \rightarrow \pi^\pm \ell^\mp \nu$. The gray region indicates the $K \rightarrow \pi W$ vertex structure.

electron mode $K_L \rightarrow \pi^\pm e^\mp \nu$ only one form factor is involved. In the following we will use the notation shown in Fig. 1, in which P , p , k and k' are the kaon, pion, electron and neutrino momenta, respectively; m is the mass of the charged pion and M that of the neutral kaon. Terms in $(P - p)_\mu$ that acquire factor of m_e are neglected. Therefore:

$$\langle \pi | J_\mu^V | K \rangle = f_+(t) (P + p)_\mu$$

We replace the form factor above with $f_+(0) \hat{f}_+(t)$, where $t = (P - p)^2 = (k + k')^2 = M^2 + m^2 - 2ME_\pi$ is the only L -invariant variable and $\hat{f}_+(0) = 1$. The form factor is dominated by the vector K - π resonances, the closest being the $K^*(892)$. Note that for $t > 0$, $\hat{f}_+(t) > 1$. The presence of the form factor increases the value of the phase-space integral and the decay rate. The natural form for $\hat{f}_+(t)$ is

$$\hat{f}_+(t) = \frac{M_V^2}{M_V^2 - t}. \quad (1)$$

It is also customary to expand the form factor as

$$\hat{f}_+(t) = 1 + \lambda'_+ \frac{t}{m^2} + \frac{1}{2} \lambda''_+ \left(\frac{t}{m^2} \right)^2 + \dots \quad (2)$$

In the following we retain linear and quadratic terms. Note that the expansion of the pole form above gives $\lambda'_+ = (m/M_V)^2$ and $\lambda''_+ = 2 \lambda'_+{}^2$. From $P + p =$

$2P - (k + k')$, and neglecting the $k + k'$ term which is also proportional to m_e , the amplitude is:

$$\mathfrak{M} = \langle \pi e \nu | H_W | K \rangle = 2 \frac{V_{us} G_F f_+(0)}{\sqrt{2}} P_\mu \bar{u}(k) \gamma^\mu (1 - \gamma^5) u(k') \hat{f}_+(t). \quad (3)$$

Squaring, summing over spins, and integrating over all variables but the pion energy, we obtain the pion spectrum

$$g(z) \propto (z^2 - 4\alpha)^{\frac{3}{2}} \left(1 + \frac{\lambda'_+}{\alpha} (\xi - z) + \frac{\lambda''_+}{2\alpha^2} (\xi - z)^2 \right)^2$$

where $\alpha = m^2/M^2$, $\xi = 1 + \alpha$ and $z = 2 E_\pi/M$ is the normalized pion energy. The spectrum can also be written in terms of $t = m^2(\xi - z)/\alpha$ as

$$h(t) \propto \lambda^{3/2} \hat{f}_+(t)^2 \quad (4)$$

$$\lambda = t^2 - 2t(M^2 + 2m^2) + (M^2 - m^2)^2$$

2 The KLOE detector

The KLOE detector consists of a large, cylindrical drift chamber (DC), surrounded by a lead/scintillating-fiber electromagnetic calorimeter (EMC). A superconducting coil around the calorimeter provides a 0.52 T field. The drift chamber [1] is 4 m in diameter and 3.3 m long. The momentum resolution is $\sigma_{p_\perp}/p_\perp \approx 0.4\%$. Two-track vertices are reconstructed with a spatial resolution of ~ 3 mm. The calorimeter [2] is divided into a barrel and two endcaps. It covers 98% of the solid angle. Cells close in time and space are grouped into calorimeter clusters. The energy and time resolutions are $\sigma_E/E = 5.7\%/\sqrt{E \text{ (GeV)}}$ and $\sigma_t = 57 \text{ ps}/\sqrt{E \text{ (GeV)}} \oplus 100 \text{ ps}$, respectively. The KLOE trigger [3] uses calorimeter and chamber information. For this analysis, only the calorimeter signals are used. Two energy deposition above threshold ($E > 50$ MeV for the barrel and $E > 150$ MeV for the endcaps) are required. Recognition and rejection of cosmic-ray events is also performed at the trigger level. Events with two energy deposition above a 30 MeV threshold in the outermost calorimeter plane are rejected.

3 Analysis

The 328 pb^{-1} of 2001-2002 data used in this analysis [4], is divided into 14 periods of about 25 pb^{-1} /period. For each data period we have a corresponding sample of Monte Carlo events with approximately the same statistics.

Candidate K_L events are tagged by the presence of a $K_S \rightarrow \pi^+\pi^-$ decay. The K_L tagging algorithm is fully described in [5] and [6]. The K_L momentum, p_{K_L} , is obtained from the kinematics of the $\phi \rightarrow K_S K_L$ decay, using the K_S direction reconstructed from the measured momenta of the decay tracks and the known value of \mathbf{p}_ϕ . The resolution is dominated by the beam-energy spread, and amounts to about 0.8 MeV/c. The position of the ϕ production point, \mathbf{x}_ϕ , is determined as the point of closest approach of the K_S , propagated backward from the K_S vertex, to the beam line. The K_L line of flight (*tagging line*) is then constructed from the K_L momentum, $\mathbf{p}_{K_L} = \mathbf{p}_\phi - \mathbf{p}_{K_S}$, and the position of the production vertex, \mathbf{x}_ϕ .

The efficiency of the tagging procedure depends slightly on the evolution of the K_L , mainly because the trigger efficiency depends on the K_L behavior. To identify events in which the K_S by itself satisfies the calorimeter trigger, we require the presence of two clusters from the $K_S \rightarrow \pi^+\pi^-$ decay associated with fired trigger sectors (*autotrigger*). The value of the tagging efficiency obtained from Monte Carlo is about 40 % and is independent of t to within 0.4%.

All tracks in the chamber, after removal of those from the K_S decay and their descendants, are extrapolated to their points of closest approach to the tagging line. For each track candidate, we evaluate the point of closest approach to the tagging line, \mathbf{x}_c , and the distance of closest approach, d_c . The momentum \mathbf{p}_c of the track at \mathbf{x}_c and the extrapolation length l_c are also computed. Tracks satisfying $d_c < ar_{xy} + b$, with $a = 0.03$ and $b = 3$ cm, and $-20 \text{ cm} < l_c < 25$ cm are accepted as K_L decay products, where r_{xy} is the distance of the vertex from the origin in the transverse plane. For each sign of charge we consider the track with the smallest value of d_c to be associated to the K_L decay. Starting from these track candidates a vertex is reconstructed. The combined tracking and vertexing efficiency for K_{e3} decays is about 54%. It is determined from data as described in Ref. 5. An event is retained if the vertex is in the fiducial volume $35 < r_{xy} < 150$ cm and $|z| < 120$ cm.

To remove background from $K_L \rightarrow \pi^+\pi^-\pi^0$ and $K_L \rightarrow \pi^+\pi^-$ decays with minimal efficiency loss, we apply loose kinematic cuts: assuming the two tracks to have the pion mass, we require $E_{miss}^2 - p_{miss}^2 - M_{\pi^0}^2 < -5000 \text{ MeV}^2$ and $\sqrt{E_{miss}^2 + p_{miss}^2} > 10 \text{ MeV}$, where E_{miss} and p_{miss} are the missing energy and momentum, respectively. A large amount of background from $K_L \rightarrow \pi\mu\nu$ decays is rejected using $\Delta_{\pi\mu}$, the lesser value of $|E_{miss} - p_{miss}|$ calculated in the two hypotheses, $\pi\mu$ or $\mu\pi$. We retain events only if this variable is greater than 10 MeV. After the kinematic cuts described above, the efficiency for the signal is about 96%.

These kinematic criteria do not provide enough suppression of the background from $K_L \rightarrow \pi^\pm e^\mp \nu$ decays with incorrect charge assignment and from

$K_L \rightarrow \pi\mu\nu$ decays. We make use of time-of-flight (TOF) information to further reduce the contamination.

For the purpose of track-to-cluster association, we define two quantities related to the distance between the track, extrapolated to the entry point of the calorimeter, and the closest cluster: d_{TC} , the distance from the extrapolated entry point on the calorimeter to the cluster centroid and $d_{\text{TC}\perp}$, the component of this distance in the plane transverse to the momentum of the track at the entry position. We only consider clusters with $d_{\text{TC}\perp} < 30$ cm and $E > 50$ MeV.

We evaluate the cluster efficiency using the Monte Carlo, and correct it with the ratio of data and Monte Carlo efficiencies obtained from control samples. A sample of K_{e3} events with a purity of 99.5% is selected by means of kinematics and independent calorimeter information. Figure 2 shows the corrections as a function of t obtained for a single run period. It is worth emphasizing that

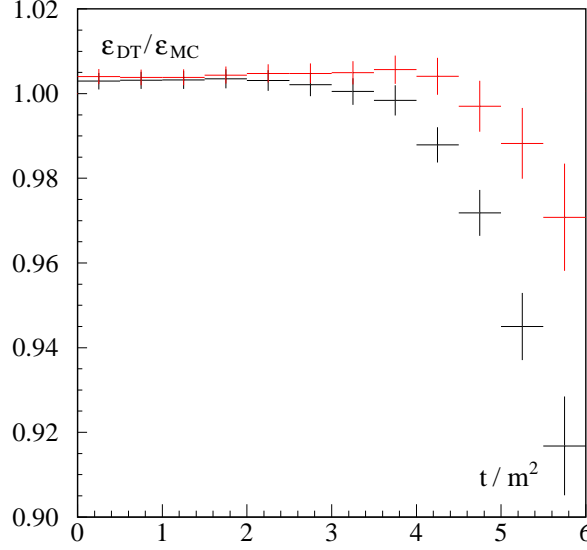


Fig. 2. Cluster efficiency correction for pions (π^- in red, π^+ in black) on the end cap from control sample. The plot refers to a single period of data taking

if this correction were not taken into account, the effect on λ'_+ would be large (about 20%) and would produce different results for each charge (about 15%). For this reason, the analysis is performed separately for each charge. The comparison of the two results provides a first check of the validity of the corrections.

For each K_L decay track with an associated cluster, we define the variable: $\Delta t_i = t_{\text{cl}} - t_i$, ($i = \pi, e$) in which t_{cl} is the cluster time and t_i is the expected time of flight, evaluated according to a well-defined mass hypothesis. The evaluating of t_i includes the propagation time from the entry point to the cluster centroid [7]. We determine the e^+e^- collision time, t_0 , using the clusters from the K_S .

An effective way to select the correct mass assignment, πe or $e\pi$, is obtained by choosing the lesser of $|\Delta t_{\pi+} - \Delta t_{e-}|$ and $|\Delta t_{\pi-} - \Delta t_{e+}|$. After the mass assignment has been made, we consider the variables $\Delta t_{\pi} + \Delta t_e$ and $\Delta t_{\pi} - \Delta t_e$. These are shown in Fig. 3 for signal and background Monte Carlo events. We select the signal by using a 2σ cut, where the resolution $\sigma \simeq 0.5$ ns. After the

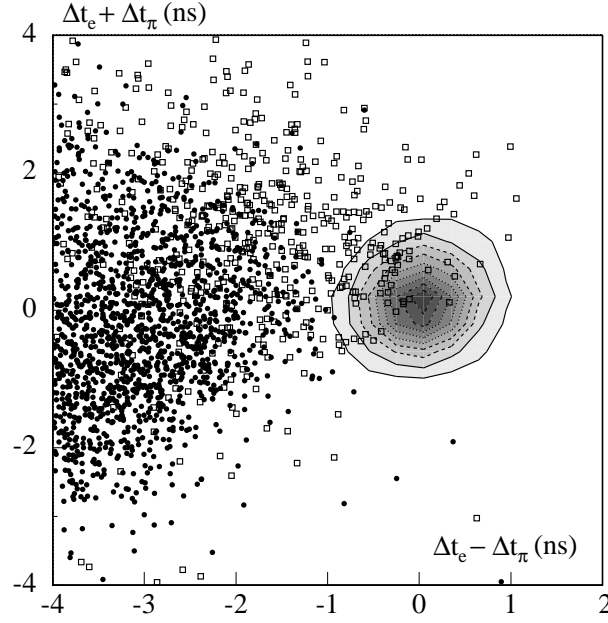


Fig. 3. Monte Carlo distribution of $\Delta t_e + \Delta t_{\pi}$ versus $\Delta t_e - \Delta t_{\pi}$. Signal (gray scale), background from opposite sign $K_L \rightarrow \pi^{\pm}e^{\mp}\nu$ (black dot), background from same sign $K_L \rightarrow \pi\mu\nu$ (empty box).

TOF cut we have a contamination of $\sim 0.7\%$, almost entirely due to $K_L \rightarrow \pi\mu\nu$ decays.

We take the TOF efficiency from the Monte Carlo after correcting the time response of the calorimeter using data control samples [7]. The quality of this correction can be checked by comparing the data and Monte Carlo distributions for Δt_e and Δt_{π} shown in Fig. 4, obtained from the same control sample used for the cluster efficiency.

We measure the form-factor slope parameters by fitting the distribution of the selected events in t/m^2 . We modify the kinematic range of t/m^2 , varying from $(m_e/m)^2 \sim 10^{-5}$ up to $(M - m)^2/m^2 \sim 6.8$, to $[-0.5, 6]$, to take into account the smearing effect at $t \sim 0$ and the low statistics at high values of t . After subtracting the residual background as estimated from Monte Carlo, we perform the fit using the following formula:

$$\frac{dN}{dt}(i) = N_0 \sum_{j=1}^{20} A(i, j) \times \rho(j, \lambda'_+, \lambda''_+) \times \epsilon_{tot}(j) \times F_{FSR}(j) \quad (5)$$

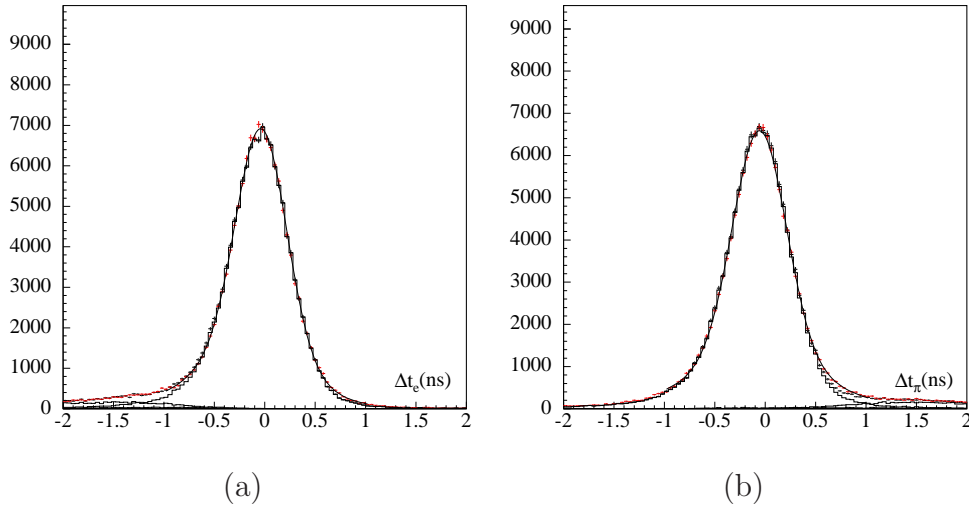


Fig. 4. Δt_i for electron (a) and pion (b) for data (black) and Monte Carlo (red)

where $\rho(j, \lambda'_+, \lambda''_+)$ is the three-body differential decay width as defined in Eq. (4), and $A(i, j)$ is the probability that an event with true value of t/m^2 in the j^{th} bin has a reconstructed value in the i^{th} bin. The chosen bin size is 0.5, which corresponds to about $1.6 \sigma_t$, where σ_t is the resolution in t/m^2 .

The total efficiency, $\epsilon_{\text{tot}}(t)$, takes into account the acceptance and the efficiency of the analysis cuts. F_{FSR} is the correction for final-state radiation. It is evaluated using the KLOE Monte Carlo simulation, GEANFI [8], where FSR processes are simulated according the procedures described in Ref. 9. FSR affects the t -distribution mainly for high-energy pions, *i.e.* for low t , where the correction is 3-5%. The slopes λ'_+ and λ''_+ are free parameters in the fit while the N_0 constant is the total number of signal events.

4 Systematic uncertainties

The systematic errors due to the evaluation of corrections, data-Monte Carlo inconsistencies, result stability, momentum miscalibration, and background contamination are summarized in Table 1.

We evaluate the systematic uncertainty of the tagging efficiency by repeating the measurement using a tagging algorithm without the requirement of the autotrigger. We observe a change of 0.14×10^{-3} for λ_+ in the case of the linear fit, and changes of 0.18×10^{-3} and 0.02×10^{-3} for λ'_+ and λ''_+ respectively for the quadratic fit.

We evaluate the systematic uncertainties on the tracking efficiency corrections by checking stability of the result when the track selection criteria are modified. We establish the validity of the method by comparing the efficiencies from

	Linear fit	Quadratic fit	
Source	$\delta\lambda_+ \times 10^3$	$\delta\lambda'_+ \times 10^3$	$\delta\lambda''_+ \times 10^3$
Tagging	0.14	0.18	0.02
Tracking and vertexing	0.16	0.22	0.18
Clustering	0.07	0.24	0.13
Time-of-flight	0.29	0.87	0.27
Background	0.08	0.16	0.03
Momentum-scale	0.06	0.05	0.05
Momentum-resolution	0.17	0.22	0.19
Total systematic	0.42	0.98	0.39

Table 1

Summary of systematic uncertainties on λ_+ , λ'_+ and λ''_+ .

data and Monte Carlo control samples, and from the Monte Carlo truth [7]. The uncertainty on the tracking efficiency correction is dominated by sample statistics and by the variation of the results observed using different criteria to identify tracks from K_L decays. The correction is run-period dependent; its statistical error is taken into account in the fit. We study the effect of differences in the resolution with which the variable d_c is reconstructed in data and in Monte Carlo events, and the possible bias introduced in the selection of the control sample, by varying the values of the cuts made on this variable when associating tracks to K_L vertices. For each variation, corresponding to a maximal change of the tracking efficiency of about $\pm 15\%$, we evaluate the complete tracking-efficiency correction and measure the slope parameters. We observe a change of 0.16×10^{-3} for λ_+ in the case of the linear fit, and changes of 0.22×10^{-3} and 0.18×10^{-3} for λ'_+ and λ''_+ , respectively, for the quadratic fit. We find a smaller uncertainty by comparing the efficiencies from data and Monte Carlo control samples, and Monte Carlo truth. However, we conservatively assume the systematic uncertainty to be given by the changes in the result observed by varying the cut on d_c .

We evaluate the systematic uncertainties on the clustering efficiency corrections by checking stability of the result when the track-to-cluster association criteria are modified. In this case as well, the uncertainties on the clustering efficiency corrections are dominated by sample statistics and by the variation of the results observed using different criteria for the track-to-cluster association. The correction is run-period dependent; we take into account its statistical error in the fit. The most effective variable in the definition of track-to-cluster association is the transverse distance, $d_{TC\perp}$. We vary the cut on $d_{TC\perp}$ in a wide range from 7 cm to 30 cm, corresponding to a change in efficiency of about 17%. For each configuration, we obtain the complete track extrapolation and

clustering efficiency correction and use it to evaluate the slopes. We observe a variation of 0.07×10^{-3} for λ_+ in the case of the linear fit, and variations of 0.24×10^{-3} and 0.13×10^{-3} for λ'_+ and λ''_+ , respectively, in the case of the quadratic fit. We find a comparable uncertainty for λ'_+ and for λ''_+ by comparing the efficiencies from data and Monte Carlo control samples, and the Monte Carlo truth.

We study the uncertainty on the Monte Carlo efficiency of the TOF selection procedure by measuring it using a pure K_{e3} control sample, and using the ratio of data and Monte Carlo efficiencies estimated in this way as a correction.¹ The control sample is selected using tighter kinematic cuts and the calorimeter particle identification described in Ref. 5. The contamination of the control sample amounts to 0.4%. When applying the correction, we find a change in the result of 0.29×10^{-3} for λ_+ in the case of the linear fit, and changes of 0.87×10^{-3} and 0.27×10^{-3} for λ'_+ and λ''_+ , respectively, in the case of the quadratic fit. These variations are well within the statistical uncertainties.

We study the uncertainties on the background evaluation by repeating the measurement on a sample with reduced background contamination. This is achieved by identifying the electron using the energy deposition in the calorimeter combined with a neural network (NN). In Fig. 5 we show the distribution of the NN output for the sample used in the analysis. Requiring the value of the NN output to be greater than 0.4, we reduce the background contamination by about a factor of three. The differences in the result obtained with this cut are 0.08×10^{-3} for λ_+ in the case of the linear fit, and 0.16×10^{-3} and 0.03×10^{-3} for λ'_+ and λ''_+ , respectively, in the case of the quadratic fit.

The effect of the momentum scale uncertainty and the momentum resolution have also been considered. We find the following relations by changing the momentum scale:

$$\frac{\delta \lambda'_+}{\lambda'_+} \simeq -2 \frac{\delta p}{p}, \quad \frac{\delta \lambda''_+}{\lambda''_+} \simeq -4 \frac{\delta p}{p}$$

We conservatively assume a momentum scale uncertainty of 0.1%, which is much greater than the value obtained from a dedicated analysis [10]. This translates into a change of 0.06×10^{-3} for λ_+ in the case of the linear fit, and changes of 0.05×10^{-3} and 0.05×10^{-3} for λ'_+ and λ''_+ , respectively, in the case of the quadratic fit.

We investigate the effect of the momentum resolution by changing the value of the resolution on t/m^2 . A variation of 3% worsens the fit quality, giving a χ^2

¹ The TOF corrections cannot be used directly in the analysis because of the correlation between the energy response in the calorimeter and the TOF.

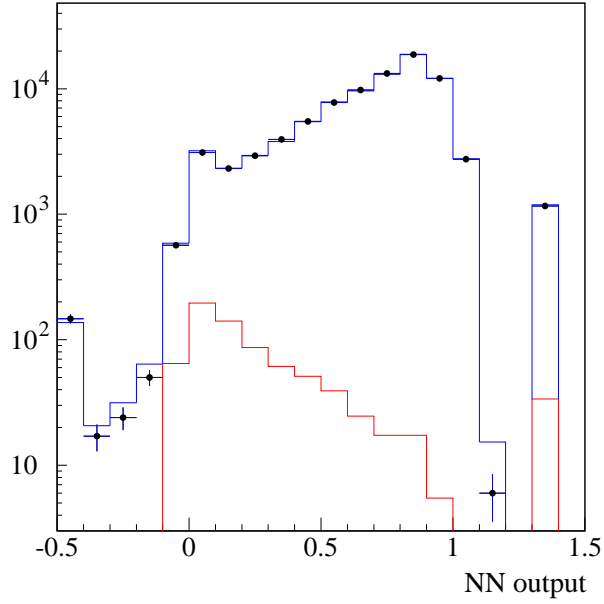


Fig. 5. NN output distribution for data (dots), Monte Carlo signal (black solid line) and background (red solid line).

probability variation of one standard deviation. The corresponding absolute changes are 0.17×10^{-3} for λ_+ in the case of the linear fit, and 0.22×10^{-3} and 0.19×10^{-3} for λ'_+ and λ''_+ in the case of quadratic fit. Varying the resolution of t/m^2 by a larger amount (6%) gives an unacceptable χ^2 probability, about 10^{-9} , while nearly the same variations for the fit parameters are observed. In principle, if the distribution has a linear behavior, the slope is insensitive to any smearing due to the resolution. The only effect is due to the depletion of the bins at the boundary of the distribution, which worsens the χ^2 of the fit. We have verified that the sensitivity to the momentum resolution is much smaller for a reduced fit range.

5 Results

About 2 million K_{e3} events were selected. The results of the linear fit obtained from all run periods are given in Table 2. The fit is performed separately for $K_L \rightarrow \pi^+ e^- \bar{\nu}$ and $K_L \rightarrow \pi^- e^+ \nu$ events to check the reliability of the evaluation of the cluster efficiency. The results are consistent only if the respective efficiency corrections for each pion charge are applied. Then, combining the two charge results and including the systematic uncertainties listed in Table 1 we obtain:

$$\lambda_+ = (28.6 \pm 0.5_{\text{stat.}} \pm 0.4_{\text{syst.}}) \times 10^{-3}$$

The results obtained for the quadratic fit are given in Table 3. A correlation of ~ -0.95 between the λ'_+ and λ''_+ parameters is obtained, as expected from the form of the parametrization in Eq. (2). A very slight preference for a small quadratic term is observed as indicated by the small improvement in the fit probability going from the linear, $P(\chi^2) = 89\%$, to the quadratic fit $P(\chi^2) = 92\%$. Including the systematic uncertainties listed in Table 1 we obtain:

$$\lambda'_+ = (25.5 \pm 1.5_{\text{stat.}} \pm 1.0_{\text{syst.}}) \times 10^{-3}$$

$$\lambda''_+ = (1.4 \pm 0.7_{\text{stat.}} \pm 0.4_{\text{syst.}}) \times 10^{-3}$$

Figure 6 shows the t/m^2 distribution for the data and the fit result. The ratio data/fit is also shown.

Linear fit	$\lambda_+ \times 10^3$	χ^2/ndf
$K_L \rightarrow \pi^- e^+ \nu$	28.7 ± 0.7	156/181
$K_L \rightarrow \pi^+ e^- \bar{\nu}$	28.5 ± 0.6	174/181
Combined	28.6 ± 0.5	330/363

Table 2

Fit results in the hypothesis $\lambda''_+ = 0$. Only statistical errors are shown.

Quadratic fit	$\lambda'_+ \times 10^3$	$\lambda''_+ \times 10^3$	χ^2/ndf
$K_L \rightarrow \pi^- e^+ \nu$	24.6 ± 2.1	1.9 ± 1.0	152/180
$K_L \rightarrow \pi^+ e^- \bar{\nu}$	26.4 ± 2.1	1.0 ± 1.0	173/180
Combined	25.5 ± 1.5	1.4 ± 0.7	325/362

Table 3

Fit results with λ'_+ and λ''_+ as free parameters. Only statistical errors are shown.

We also fit the data using the one-pole parametrization (see Eq. (1)). We obtain $M_V = (870 \pm 6) \text{ MeV}$ with $\chi^2/\text{ndf} = 326/364$ and a probability of $P(\chi^2) = 92.4\%$. Taking the systematic error into account, we obtain:

$$M_V = (870 \pm 6_{\text{stat.}} \pm 7_{\text{syst.}}) \text{ MeV}$$

This result indicates that, although the pole is dominated by the K^* vector meson, contributions from other $J^P = 1^-$ resonant and non-resonant $K\pi$ scattering amplitudes are not negligible.

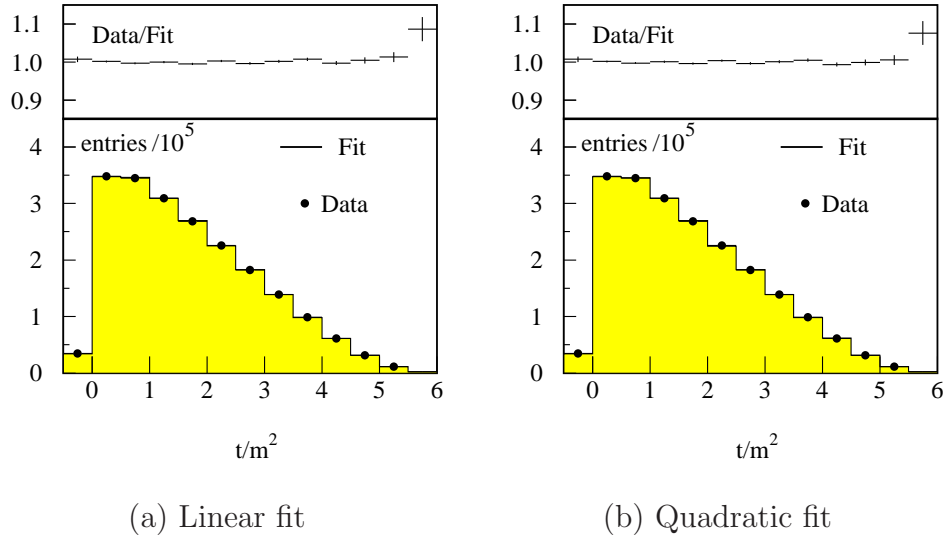


Fig. 6. Fit results: data (dots) are superimposed on the fit function (histogram). The data/Fit ratio is also shown.

Conclusion

We have obtained precise new values of the slopes used to describe the hadronic form factor in K_{e3} decay. The new KLOE result is consistent with the presence of a small quadratic term in agreement with the expectation of the one-pole expansion. The value of λ_+ obtained with the linear fit is in good agreement with other existing measurements. The comparison with other existing measurements is shown in Fig. 7 in the case of the quadratic fit. Our result is in good agreement with ISTRAP+ [11] and NA48 [12] and in marginal disagreement with KTeV [13].

Acknowledgements

We thank the DAΦNE team for their efforts in maintaining low background running conditions and their collaboration during all data-taking. We want to thank our technical staff: G.F.Fortugno for his dedicated work to ensure an efficient operation of the KLOE Computing Center; M.Anelli for his continuous support to the gas system and the safety of the detector; A.Balla, M.Gatta, G.Corradi and G.Papalino for the maintenance of the electronics; M.Santoni, G.Paoluzzi and R.Rosellini for the general support to the detector; C.Piscitelli for his help during major maintenance periods. This work was supported in part by DOE grant DE-FG-02-97ER41027; by EURODAPHNE, contract FMRX-CT98-0169; by the German Federal Ministry of Education and Research (BMBF) contract 06-KA-957; by Graduiertenkolleg ‘H.E. Phys.

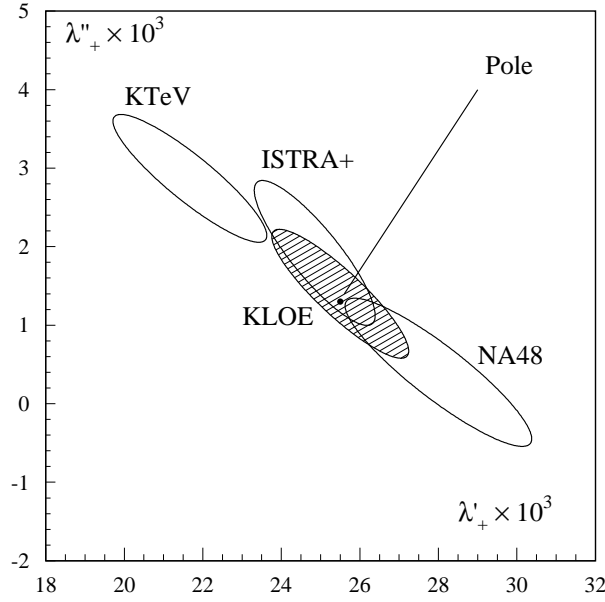


Fig. 7. Comparison of present results with other recent measurements [11–13]. The black dot represents the values of λ'_+ and λ''_+ obtained from the Taylor expansion of the pole parametrization. The ISTRA+ result is corrected with the ratio $(m_{\pi^+}/m_{\pi^0})^2$.

and Part. Astrophys.' of Deutsche Forschungsgemeinschaft, Contract No. GK 742; by INTAS, contracts 96-624, 99-37; by TARI, contract HPRI-CT-1999-00088.

References

- [1] M. Adinolfi, et al., The tracking detector of the KLOE experiment, Nucl. Instrum. Meth. A 488 (2002) 51.
- [2] M. Adinolfi, et al., The KLOE electromagnetic calorimeter, Nucl. Instrum. Meth. A 482 (2002) 364.
- [3] M. Adinolfi, et al., The trigger system of the KLOE experiment, Nucl. Instrum. Meth. A 492 (2002) 134.
- [4] M. Antonelli, M. Dreucci, C. Gatti, Measurement of the K_{e3} Semileptonic Form Factor Slope and Curvature and Pole in the Decay $K_L \rightarrow \pi e \nu$ at KLOE, KLOE Note 210 (2006).
URL <http://www.lnf.infn.it/kloe/pub/knote/kn210.ps>
- [5] M. Antonelli, P. Beltrame, M. Dreucci, M. Moulson, M. Paultan, A. Sibidanov, Measurements of the Absolute Branching Ratios for Dominant K_L Decays, the K_L Lifetime, and V_{us} with the Kloe Detector, KLOE Note 204 (2005).
URL <http://www.lnf.infn.it/kloe/pub/knote/kn204.ps.gz>

- [6] KLOE Collaboration, F. Ambrosino, et al., Phys. Lett. B 632 (2006) 43.
- [7] KLOE Collaboration, F. Ambrosino, et al., Measurement of the branching fraction and charge asymmetry for the decay $K_S \rightarrow \pi e \nu$ with the KLOE detector, hep-ex/0601026, Submitted to Phys. Lett. B, and references therein .
- [8] F. Ambrosino, et al., Data handling, reconstruction, and simulation for the KLOE experiment, Nucl. Instrum. Meth. A 534 (2004) 403.
- [9] C. Gatti, Monte Carlo simulation for radiative kaon decays, hep-ph/0507280, accepted by Eur. Phys. J. C, and references therein .
- [10] A. Antonelli, et al., The KLOE field map revisited, KLOE Memo 233 (2001).
- [11] O. P. Yushchenko, et al., Phys. Lett. B 589 (2004) 111.
- [12] NA48 Collaboration, A. Lai, et al., Phys. Lett. B 606 (2004) 1.
- [13] KTeV Collaboration, T. Alexopolous, et al., Phys. Rev. D 70 (2004) 092007.